Mon. Not. R. Astron. Soc. **273,** 945–957 (1995)

Simulations of starburst spectral evolution superimposed on old populations: extension to dwarf ellipticals

Alex A. Schmidt,[1] Danielle Alloin[2] and Eduardo Bica[3]

[1] *Departamento de Matemática e NEPAE, Universidade Federal de Santa Maria, 97119-900 Santa Maria, RS, Brazil*
[2] *Observatoire de Paris, DAEC, URA 173 CNRS, F-92195, Meudon, France*
[3] *Departamento de Astronomia, IF-UFRGS, CP 15051, 91501-970 Porto Alegre, RS, Brazil*

Accepted 1994 November 3. Received 1994 October 4; in original form 1994 January 4

ABSTRACT

In order to gain a better understanding of starburst and merger events, we have extended to dwarf galaxies our previous spectral simulations of burst evolution over 3 Gyr, superimposed on an old underlying stellar population. We have used a library of star cluster and galaxy integrated spectra in the 3700–9700 Å wavelength range. Two kinds of galaxy spectra representing the underlying red stellar populations have been considered: (i) an average spectrum of the central regions of NGC 3056 and 4476, for which previous population syntheses have shown a maximum metallicity of $[Z/Z_{\odot}] = -0.5$, and (ii) a combination of globular cluster spectra in the range $-2 \leq [Z/Z_{\odot}] \leq -1$, which could represent the old stellar population in the transition between dwarf ellipticals and dwarf spheroidals. These spectra were combined with those of Large Magellanic Cloud (LMC) and Galactic disc star clusters in the 3-Myr to 3-Gyr age range, in order to simulate starburst events in dwarf galaxies and model the subsequent spectral evolution of the composite system. The star cluster spectra have been properly scaled to represent starburst-to-galaxy mass fractions of 10, 1 and 0.1 per cent. The resulting models form a spectral atlas for comparisons with observations. Rest-frame *BVRI* magnitudes and the related colours have been derived from these models, as well as the equivalent widths for a set of metallic and Balmer features. The behaviour of these indices is analysed as a function of the burst age and strength. The results can be used to study the properties of star-forming events in galaxies.

Key words: galaxies: elliptical and lenticular, cD – galaxies: evolution – galaxies: starburst – galaxies: stellar content.

1 INTRODUCTION

It is quite noticeable from recent astronomical literature that there is a revival of interest in the study of dwarf galaxies. There are at least two obvious reasons for such a situation to occur: (i) the dwarf galaxy population can provide information about the galaxy formation process (Bardeen et al. 1986; Deckel & Silk 1986; Peebles 1987), and (ii) dwarf galaxies are quite numerous and, although they are not detected at large distances, they might play an important role in the evolution of clusters of galaxies.

The need to understand dwarf galaxies in the context of galaxy evolution drove us to perform the simulations presented in this paper, assuming implicitly that gravitational interactions lead to star formation, the entire process hereafter referred to as a merger event either between two dwarfs or between a dwarf and an intergalactic cloud (e.g., Larson 1987). Related to this approach also are the questions of how we could identify genuine young galaxies in the local Universe and for how long a merger event would hide the old populations in the initial merging systems.

Assuming that merging is indeed a standard process at work in galaxy clusters, it is important to find out which observational constraints are best suited for dating the merger events. Broad-band colour photometry has often been used [first by Larson & Tinsley (1978)] because such data can be easily collected for large samples of galaxies (e.g., Schweizer & Seitzer 1992 and references therein). Yet large telescopes coupled with highly sensitive detectors have come into service, so that high-quality spectra can now be obtained for similar galaxy samples.

In order to date a merger event from the composite resulting system, it should be remembered that the following parameters are of relevance: (i) the initial masses, stellar populations and dust contents of the two merging systems, which may both be composite in age and metallicity; (ii) the

mass fraction involved in the starburst induced by the merging, and (iii) the age of the starburst. This is a minimum list of parameters to be taken into account in this kind of approach, and therefore routes must be explored to ensure that an adequate number of observational inputs will be available for a diagnosis. This is why spectrophotometry, over as large a wavelength range as possible (ideally from 1200 Å up to 5 μm), measuring feature strengths and continuum distribution, is an important goal for satisfactory observation.

Modelling of starbursts induced by merger events is often performed via evolutionary syntheses which, in general, use solar-metallicity stellar spectra and/or colours in the model output for comparisons with observations (e.g., Guiderdoni & Rocca-Volmerange 1987; Yoshii & Arimoto 1987; Charlot & Bruzual 1991). The code by Yoshii & Arimoto (1987) takes some account of the full range of metallicity variation, $[Z/Z_\odot]$ from -2 up to 1. Metallicities above the solar value are not a necessary input in the case of dwarf galaxies which, as a rule, are metal-poor (Hensler, Theis & Burkert 1992). On the other hand, in the case of giant ellipticals, neglect of the large metallicity in their bulges has certainly led to some misinterpretations. In addition, the many free parameters of an evolutionary synthesis code cannot be constrained if one uses only a few broad-band photometric data points available along a galaxy spectrum.

In this paper we have followed another approach, simulating the occurrence of a starburst, represented by the integrated light of a star cluster at a given age and metallicity, in a dwarf galaxy for which two different types of stellar populations will be considered. The first type is given by the average spectrum of the low-luminosity ellipticals ($M_V \sim -18$) NGC 3056 and 4476, which attain a maximum metallicity $[Z/Z_\odot] = -0.5$ (Bica 1988), hereafter referred to as the E4 spectral template. The second is given by a mixture of globular cluster spectra in the range $-2 \leq [Z/Z_\odot] \leq -1$, intended to represent the old stellar population in objects at the transition between dwarf ellipticals and dwarf spheroidals, hereafter referred to as the dES spectral template. The main advantage of this starburst simulation approach is that both the initial mass function and the stellar evolution are implicit in the star cluster spectral data.

This paper is a companion study to that by Bica, Alloin & Schmidt (1990a) wherein we have simulated the effects of starburst evolution in two typical bulge stellar populations, one with maximum metallicity attaining the solar value and another attaining $[Z/Z_\odot] = 0.6$. For the simulation itself, in this paper we have applied the same technique, which is briefly recalled in Section 2. Our parameters are the mass percentage involved in the starburst and the burst age, which dates the star-forming event induced by the merging; therefore we can follow the spectral and colour evolution of the composite system. We recall that the details of the first few Myr of evolution are outwith the scope of this work; the emission-line phases of a starburst are studied in detail elsewhere (e.g., Terlevich 1985; Cid-Fernandes et al. 1992; and Garcia-Vargas & Díaz 1994). Our study is complementary to these studies because it follows, instead, the evolution from the starburst onwards and the impact of the starburst on the light of the composite system up to a few Gyr. In addition to the spectral evolution of the merging system, quantitative results of the simulations are provided in Section 3 for evolution of broad-band *BVRI* magnitudes and colours, and evolution of some key spectral features. Conclusions are summarized in Section 4.

2 STARBURST SIMULATIONS

The present models are built from a library of galaxy and star cluster integrated spectra in the visible and near-infrared ranges, along with the corresponding grid of spectral properties as a function of age and metallicity. The observational material consists of spectra of 12-Å resolution over a spectral range of 3700–9700 Å, collected at the European Southern Observatory, La Silla (ESO), which, together with the grid of spectral features, have been previously discussed by Bica & Alloin (1986a, b; 1987a, b).

Young and intermediate-age star clusters in the Large Magellanic Cloud (LMC), Small Magellanic Cloud (SMC) and Galactic disc are used to represent the starbursts at various ages. Therefore, the simulations will correspond to star formation events involving gas with less than or equal to the solar metallicity value. As for metal-rich burst simulations, we point out (Bica et al. 1990a) that not much difference is to be expected with the present models, since the visible spectral range of burst components for ages up to 500 Myr is practically dominated by hot stars which have quite weak or absent metal features. As introduced in Section 1, two different types of underlying galactic old stellar populations – the initially merging systems – have been considered: the E4 and the dES spectral templates. The dES stellar population template has been built from the star cluster spectral library (Bica 1988) using three Galactic globular cluster templates, G3, G4 and G5 (Bica 1988), with average metallicities $[Z/Z_\odot] = -1.0$, -1.5 and -2.0, respectively, contributing to the integrated light of dES at 5870 Å with respective percentages 55, 35 and 10 per cent. These relative contributions follow predictions of galaxy evolutionary models with supernova-driven galactic winds (Arimoto & Yoshii 1987). In the present paper, therefore, we shall essentially be modelling merger events involving systems with a low metal content. The E4 galaxy template is shown in Fig. 1(a) and the synthetic dES galaxy template is displayed in Fig. 1(b), together with the individual globular cluster spectral contributions used to build up this metal-poor dwarf galaxy template.

Our choice of the metallicity level for dES is meant to represent the range of chemical abundance observed in galaxies lying in the transition between dwarf ellipticals (dE) and dwarf spheroidals (dSph). Fornax, the brightest dSph in the Milky Way halo, has $M_V = -13.7$ and average $[Z/Z_\odot] \sim -1.4$ (Buonanno et al. 1985, and references therein), while the dwarf ellipticals like NGC 147, 185 and 205 (companions of M31) range in M_V from -15.1 to -16.3 and in metallicity from $[Z/Z_\odot] \sim -1$ to ~ -0.5 (Bica, Alloin & Schmidt 1990b; Lee et al. 1993). We point out that Fornax presents an intermediate-age component denoted by the occurrence of carbon stars (Azzopardi & Lequeux 1992, and references therein), and NGC 205 presents a young component (Bica et al. 1990b). Consequently, the starburst plus old population models presented below should account for such mixtures.

The flux proportions for combining the underlying stellar population (low metal content galaxy template) with a younger stellar generation (starburst at a given age) are deter-

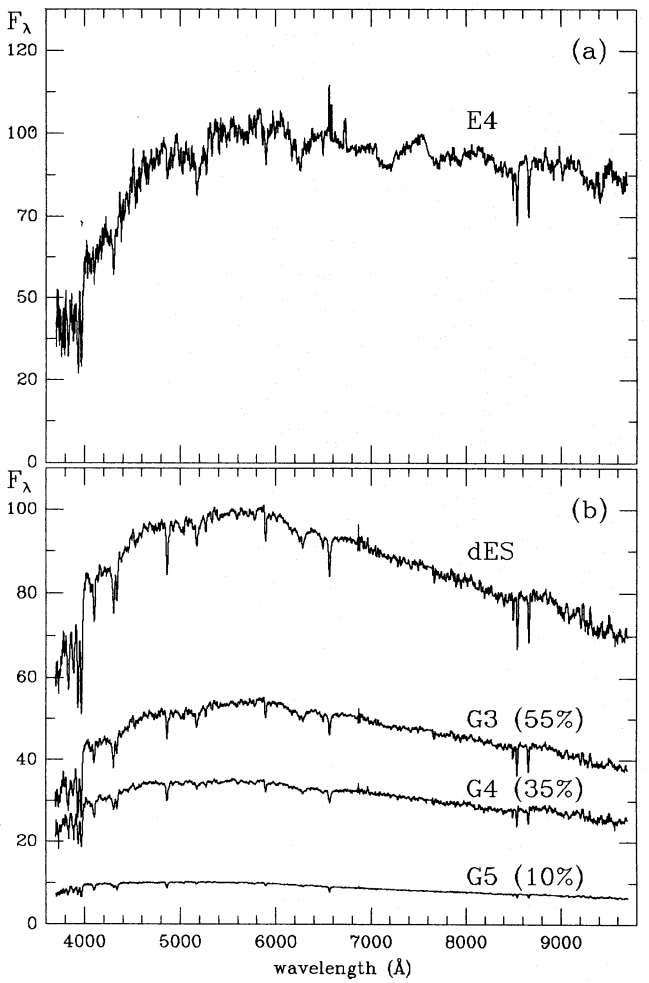

Figure 1. Spectral templates used to represent the old metal-poor stellar population of dwarf galaxies: (a) the E4 template obtained as an average spectrum of the nuclear regions of NGC 3056 and 4476, reaching $[Z/Z_\odot] = -0.5$ as described in Bica (1988); (b) the dES template intended to represent the transition between a dwarf elliptical and a dwarf spheroidal, obtained from the combination of the globular cluster templates G3 ($[Z/Z_\odot] = -1.0$), G4 ($[Z/Z_\odot] = -1.5$) and G5 ($[Z/Z_\odot] = -2.0$) of Bica (1988), respectively, with flux fractions 55, 35 and 10 per cent at 5870 Å. All spectra are normalized to 100 flux units at 5870 Å where the G3, G4 and G5 templates have been scaled according to their relative contributions to dES.

Table 1. Properties of the star cluster spectral groups.

Group	Age (Gyr)	M/L_V	$L_V/L(5870\,Å)$	$L(5870\,Å)$
RH	0.000 – 0.007	0.030	1.180	242.90
Y1	0.007 – 0.020	0.007	1.056	1163.40
Y2	0.020 – 0.070	0.054	1.168	136.40
Y3	0.070 – 0.200	0.260	1.172	28.20
Y4	0.200 – 0.700	0.310	1.105	25.10
I1	0.700 – 2.000	1.290	1.077	6.19
I2	2.000 – 7.000	3.090	1.022	2.72
G2	>10	8.600	1.000	1.00

mined by the choice of three burst-to-galaxy mass fractions, respectively, 10, 1 and 0.1 per cent. The approach to the problem of relating mass fractions to flux fractions has been made by examining the photometric evolution of a single-generation system – a star cluster – as analysed by Arimoto & Bica (1989), using the evolutionary synthesis code from Arimoto & Yoshii (1986). The evolution of the mass-to-light ratio M/L_V of this system allows the mutual transformation of population synthesis results from flux fractions to mass fractions (Bica, Arimoto & Alloin 1988). In Table 1 we recall the properties of the star cluster groups used in this analysis. The spectral group designation is shown in column 1: RH stands for an emission-line phase (in this case, a mixture of H II regions in the range 4.5–6 Myr); Y for the young groups; I for the intermediate-age groups and G for globular clusters. The related age range is given in column 2. The M/L_V ratio according to Bica et al. (1988) is provided in column 3. Column 4 displays the $L_V/L(5870\,Å)$ ratio relative to group G2, the oldest star cluster template with a metallicity comparable to that of the younger groups. This ratio is an observed quantity used to transform V fluxes mutually into our adopted monochromatic flux normalization at 5870 Å. Finally, column 5 shows the $L(5870\,Å)$ flux evolution along the age sequence shown for equal-mass groups and relative to the oldest one (G2). It should be pointed out that our star cluster theoretical models and spectral library include the red supergiant phase at about 10–15 Myr which leads to the red flux increase in group Y1. The sequence shown in Table 1 has been found to be quite suitable to model the passive flux fading of a starburst, as a result of stellar evolution. The colours and feature equivalent widths (Å) for the input systems – star clusters, E4 and dES templates – are provided in Table 2. The spectral windows of the features are defined as in Bica & Alloin (1986a, 1987b), consisting of the following: 3908–3952 Å for Ca II K; 4082–4124 Å for Hδ; 4150–4214 Å for CN4216; 4318–4364 Å for Hγ; 4846–4884 Å for Hβ; 5156–5196 Å for Mg I+MgH; 8520–8564 Å for Ca II 8542; and 8640–8700 Å for Ca II 8662.

Starburst simulations in a dwarf galaxy are produced by combining the spectrum of a chosen underlying old population (E4 or dES) with a star cluster spectrum at a given age (RH to I2), scaled with respect to the galaxy spectrum according to column 5 of Table 1 and to the burst-to-galaxy mass fraction chosen (0.1, 1 or 10 per cent). Fig. 2 shows the full evolutionary sequence of the composite spectrum for the case of a 1 per cent burst-to-galaxy mass fraction for the E4 galaxy template as the underlying old stellar population system. In Fig. 3 we provide a subset of the sequence corresponding to a 10 per cent burst-to-galaxy mass fraction, and in Fig. 4 a subset of the sequence corresponding to a 0.1 per cent burst-to-galaxy mass fraction. In each figure we have displayed the composite spectrum and either the starburst spectrum or that of the underlying dwarf galaxy, for the sake of clarity. A parallel series of evolutionary sequences is given in Figs 5, 6 and 7 for the case of the dES galaxy template as the underlying old population system.

Regardless of the underlying old stellar population, the starburst component dominates the integrated light up to 50 Myr, even for the starburst-to-galaxy mass fraction of 0.1 per cent, because of the strong light input from young blue stars and red supergiants. Later, the impact of the starburst on the

Table 2. Colours and equivalent widths (Å) derived for the galaxy and star cluster spectra.

Group	$(B-V)$	$(V-R)$	$(V-I)$	Ca II K	Hδ	CN 4216	Hγ	Hβ	Mg I+MgH	Ca II 8542	Ca II 8662
E4	0.92	0.69	1.38	13.9	4.4	3.8	4.9	3.1	6.3	5.2	4.6
dES	0.76	0.61	1.25	8.7	3.9	2.4	4.1	3.1	2.2	2.6	2.8
RH	0.18	0.41	0.18	-0.6	-12.0	0.0	-24.0	-70.5	0.0	0.0	0.0
Y1	0.36	0.50	1.31	2.0	4.2	1.8	3.3	4.1	3.0	6.4	5.5
Y2	0.24	0.30	0.68	1.3	9.1	2.2	7.0	7.1	1.6	5.9	6.2
Y3	0.25	0.27	0.64	2.4	10.0	2.9	8.6	8.0	1.7	5.8	5.6
Y4	0.46	0.41	0.83	7.1	11.6	1.3	8.3	8.5	3.0	4.4	4.9
I1	0.60	0.47	0.87	9.1	8.9	2.4	8.3	7.3	2.4	3.5	5.2
I2	0.75	0.62	1.29	11.3	7.1	4.9	6.8	5.8	2.8	4.6	5.0

composite system light can be traced through the strong series of Balmer absorption lines up to 1 Gyr, in particular in the 10 per cent burst-mass case, and by an enhancement of these lines for smaller burst contributions. The shape of the composite continuum is clearly affected by the burst (the blue component) up to 50 Myr in the 1 per cent burst-mass case, both for E4 and for dES. On the other hand, the influence of the blue continuum is still very strong at 500 Myr for the 10 per cent burst-mass case. It is interesting to note in the 0.1 per cent burst-mass sequence for the dES template (Fig. 7) that, despite the fact that the burst component fades away after 500 Myr, the spectrum remains considerably blue since the pure old population is metal-poor (Fig. 1b). Clearly, broad-band colours alone would hardly allow the latter case to be distinguished from a bluish spectrum with an important burst component in a more metal-rich system, like E4 at 100 Myr for the 1 per cent burst-mass case (Fig. 2d). Nevertheless, feature strengths should allow the disentanglement of such ambiguities between age and metallicity (Section 3).

The sequence of spectral models shown in Figs 2 to 7, together with the corresponding ones for metal-rich bulges presented in Bica et al. (1990a), can be used as a guideline spectral atlas for diagnosing age and metallicity effects of burst evolution in galaxy observations.

3 SIMULATION RESULTS

3.1 Time evolution of magnitude and colours

The simulation results can be provided in a more quantitative way by following the evolution with time of the colours of the composite system, as well as its magnitude changes. These are displayed in Table 3(a) (columns 2–8) for the case of the E4 underlying old population and Table 3(b) for the case of the dES underlying population.

The broad-band filter profiles that we have used to compute the colours and magnitude changes are from Ažhusenis & Straižhis (1969) for the B and V bands, and from Bessel & Wickramasinghe (1979) for the R and I bands. The calibration of our photometric system was made using these filter profiles on the Gunn & Stryker (1983) spectral atlas, assuming standard colours for the stars from Johnson (1964). The mean standard errors resulting from this calibration are 0.02, 0.04 and 0.07 mag respectively for $(B-V)$, $(V-R)$ and $(R-I)$. We emphasize that the present colours and those in Bica et al. (1990a) are in the Johnson (J) system. The transformation to the Johnson–Cousins (JC) system is straightforward by means of the following equations:

$$(V-R)_{JC}=0.7217(V-R)_{J}-0.0277, \quad (1)$$

$$(R-I)_{JC}=0.7726(R-I)_{J}+0.0081, \quad (2)$$

which we have derived using Johnson–Cousins colours applied to the Gunn & Stryker (1983) spectral atlas. The coefficients given above are consistent with those previously derived by Cousins (1976) and Bessel (1979).

The evolution of the magnitude changes in B, V, R and I and of the $(B-V)$, $(V-R)$, $(V-I)$ and $(R-I)$ colours as a function of the burst age and strength are shown in Figs 8 and 9, respectively, for the burst plus dES template case. The corresponding effects for the E4 case are very similar (see Table 3) and have not been displayed. The pattern of the changes in magnitude (Fig. 8), arising from the influence of the starburst, is similar in all bands displayed. The red supergiant luminosity peak at ~10 Myr is easily distinguished in the various spectral ranges, independently of the burst intensity and appears more contrasting for the redder bands. The burst detection cut-off, as a function of the burst intensity, can be easily estimated from these figures. With regard to the colour diagrams (Fig. 9), the long-lasting effects of the starburst can be better distinguished in $(B-V)$ than in $(V-R)$, as the B band is more responsive to the presence of young stars. The red supergiant effect is quite prominent as well in these colour diagrams. In particular, in the $(V-I)$ and $(R-I)$ colours the red supergiant phase is virtually independent of the burst-to-galaxy mass fractions considered. Finally, burst detection cut-offs can also be estimated from these colour diagrams.

3.2 Time evolution of key spectral features

In this section we show the evolution of a number of key spectral features particularly suited for dating merger events and/or the starburst strength, such as the Ca II K line, the CN 4216 band, the Mg I + MgH feature, the two strong lines of the Ca II infrared triplet and, of course, the Balmer lines

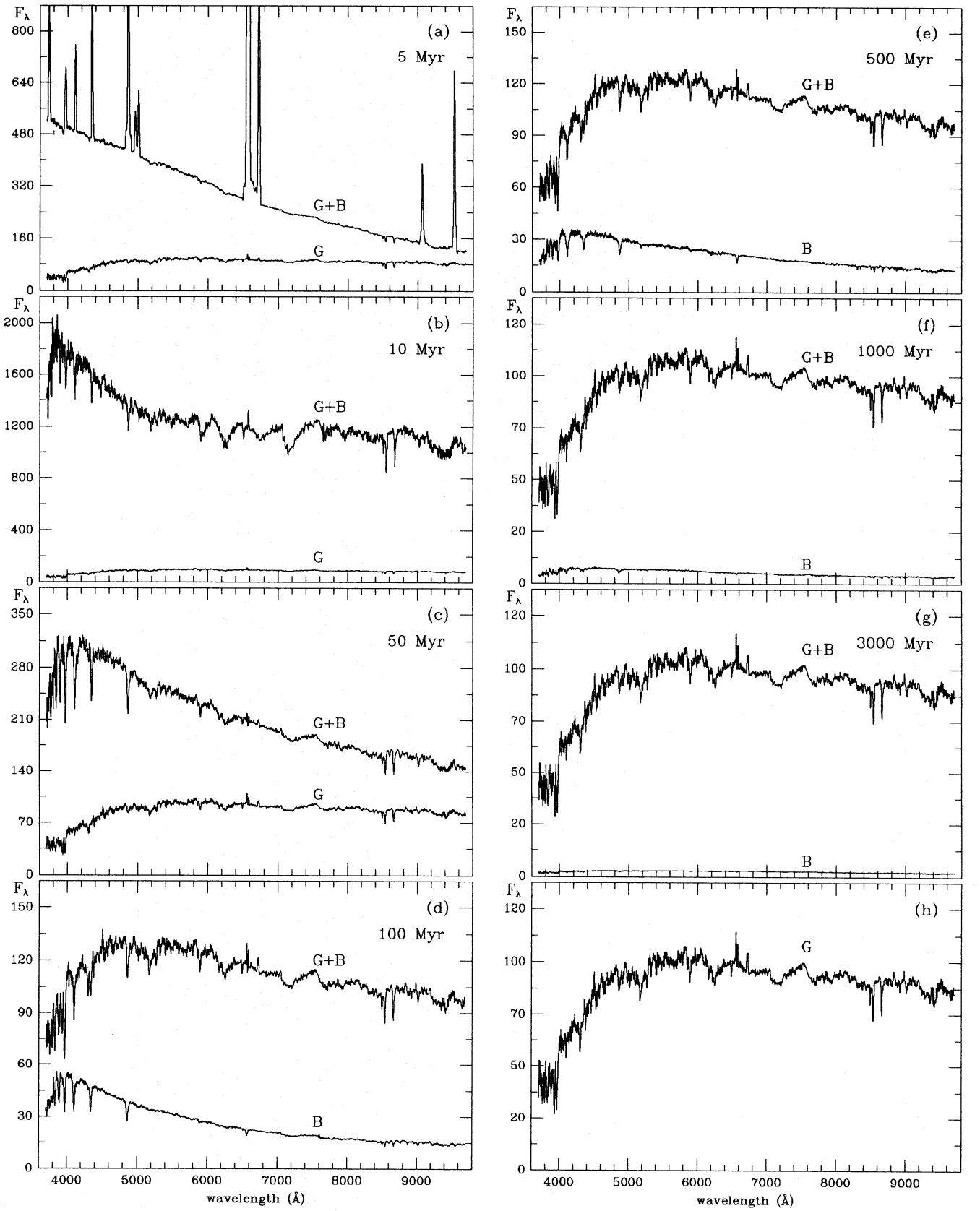

Figure 2. The galaxy-plus-burst age sequence of a burst mass fraction of 1 per cent for the E4 underlying stellar population case. In all figures, the relative intensity scale corresponds to $F_\lambda = 100$ at 5870 Å for the pure E4 spectrum. Each figure shows the composite spectrum (G + B) and either the underlying galaxy spectrum (G) or the burst spectrum (B). The burst age is indicated in the upper right corner of each figure.

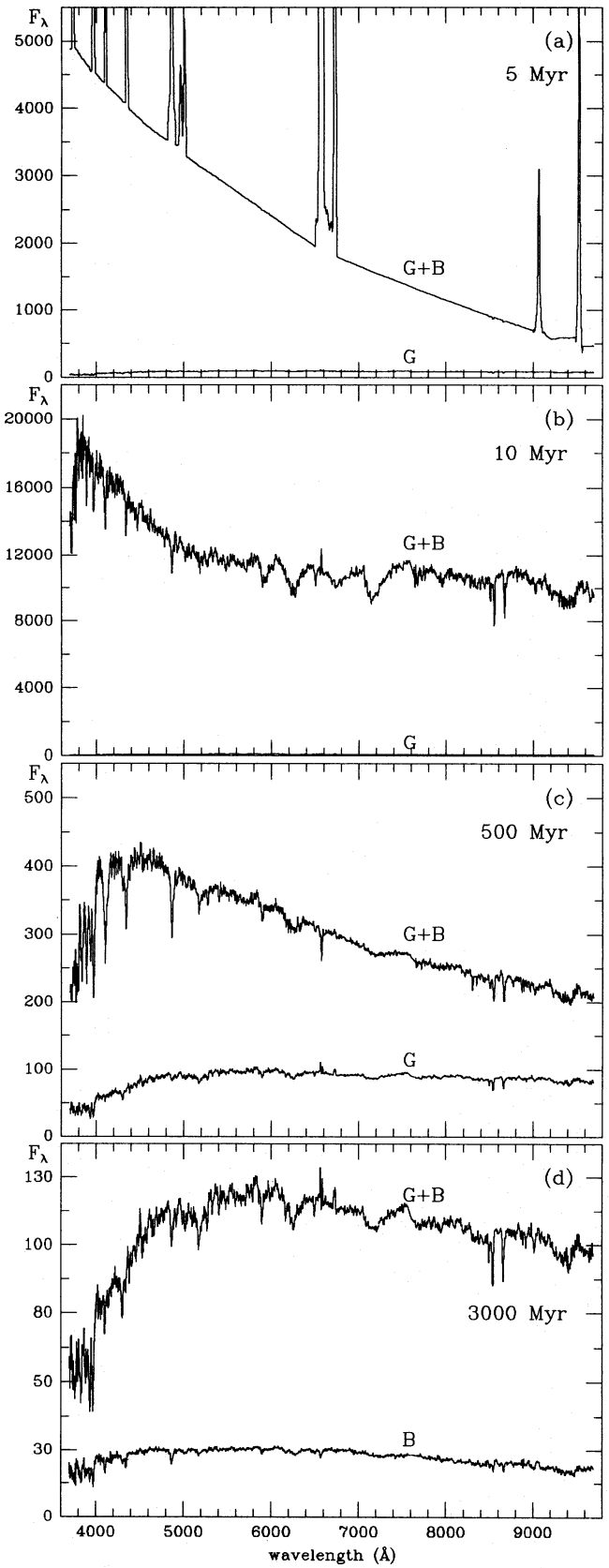

Figure 3. The effect of a 10 per cent burst mass fraction occurring in an underlying stellar population like the E4 template. Same intensity scale and notes as in Fig. 2.

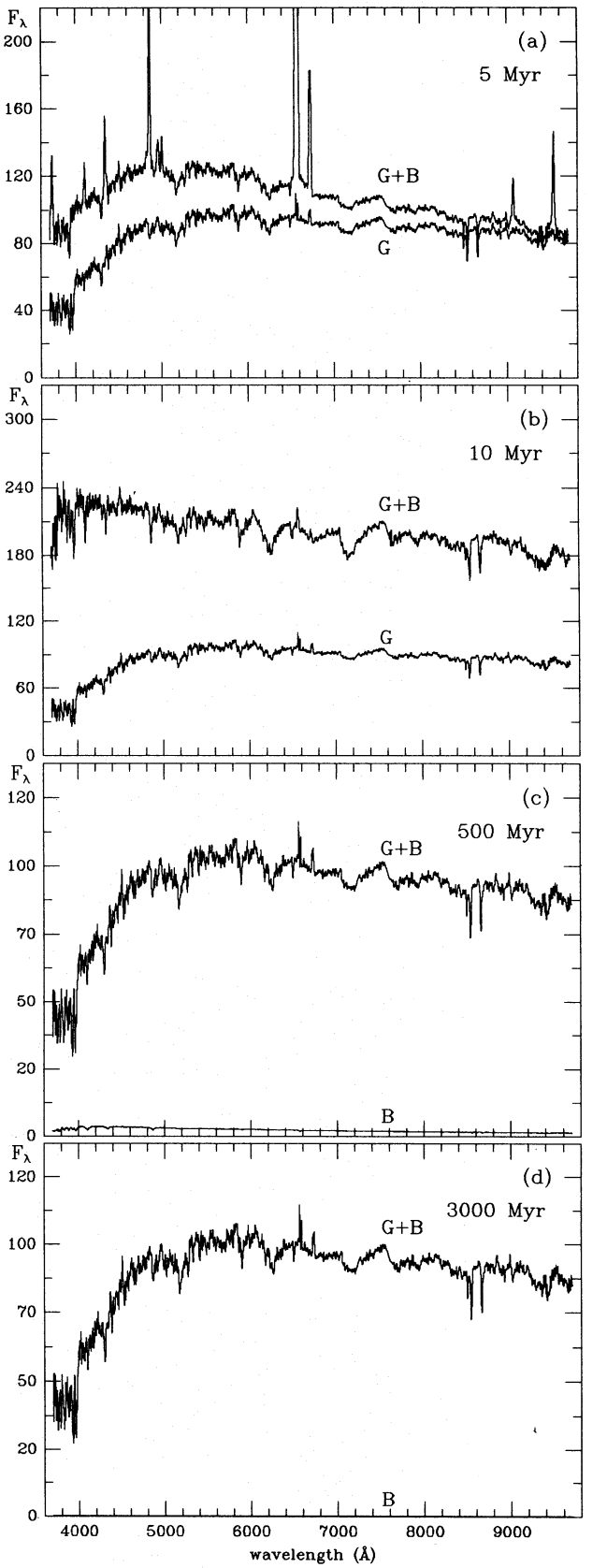

Figure 4. The effect of a 0.1 per cent burst mass fraction occurring in an underlying stellar population like the E4 template. Same intensity scale and notes as in Fig. 2.

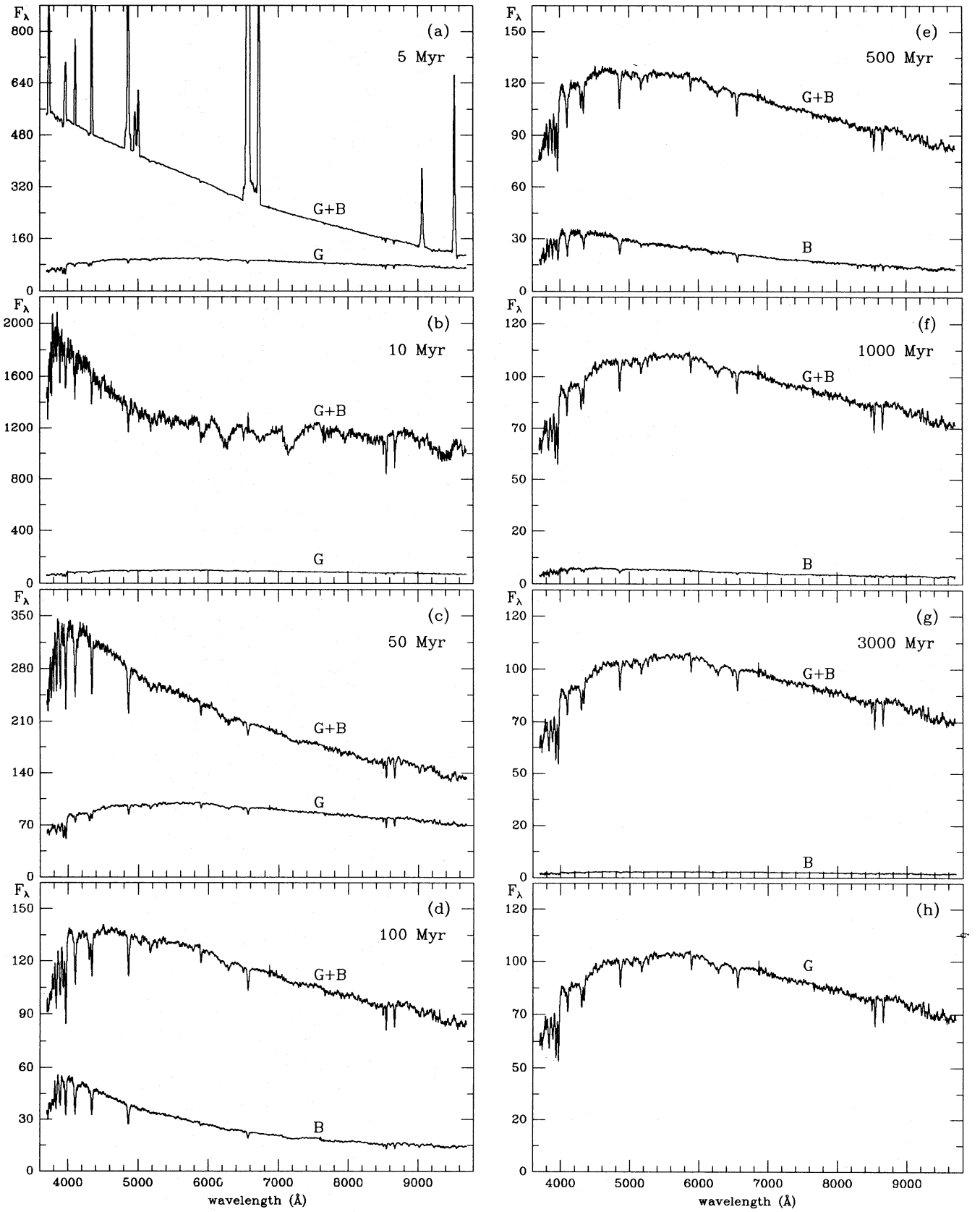

Figure 5. Same as Fig. 2 for the case of the dES template as the underlying stellar population.

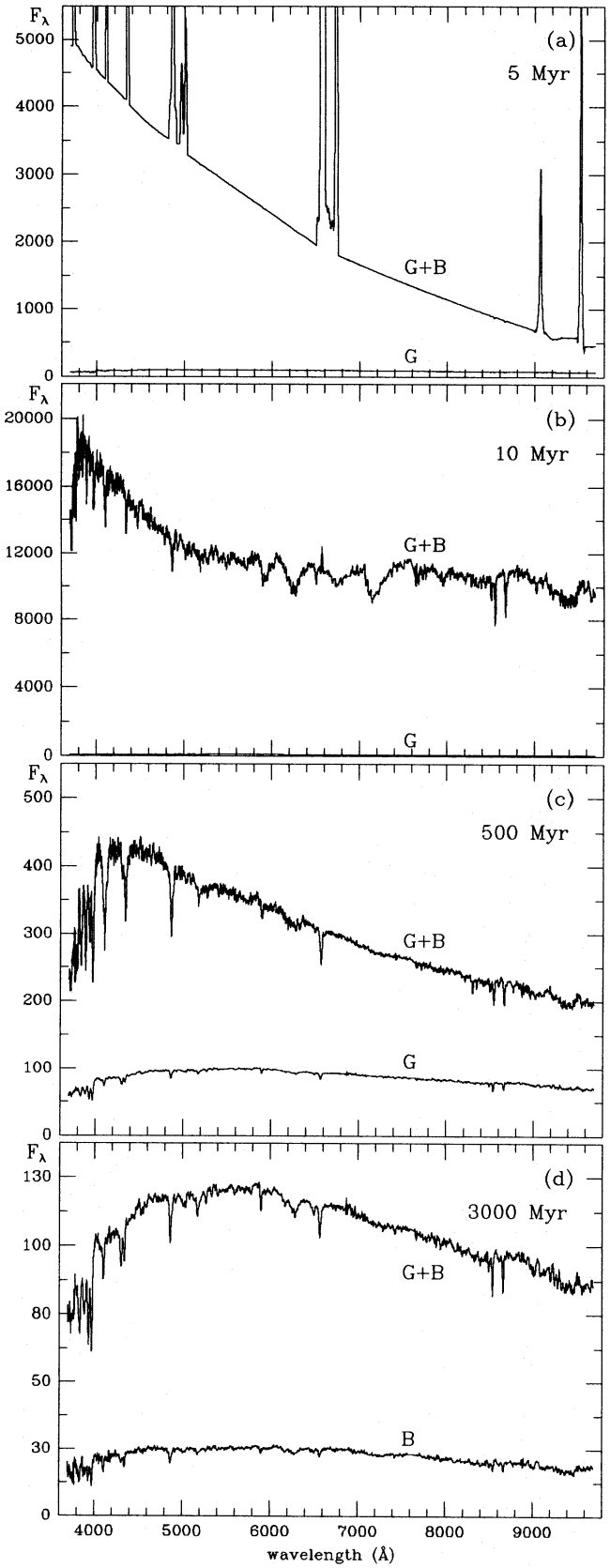

Figure 6. Same as Fig. 3 for the case of the dES template as the underlying stellar population.

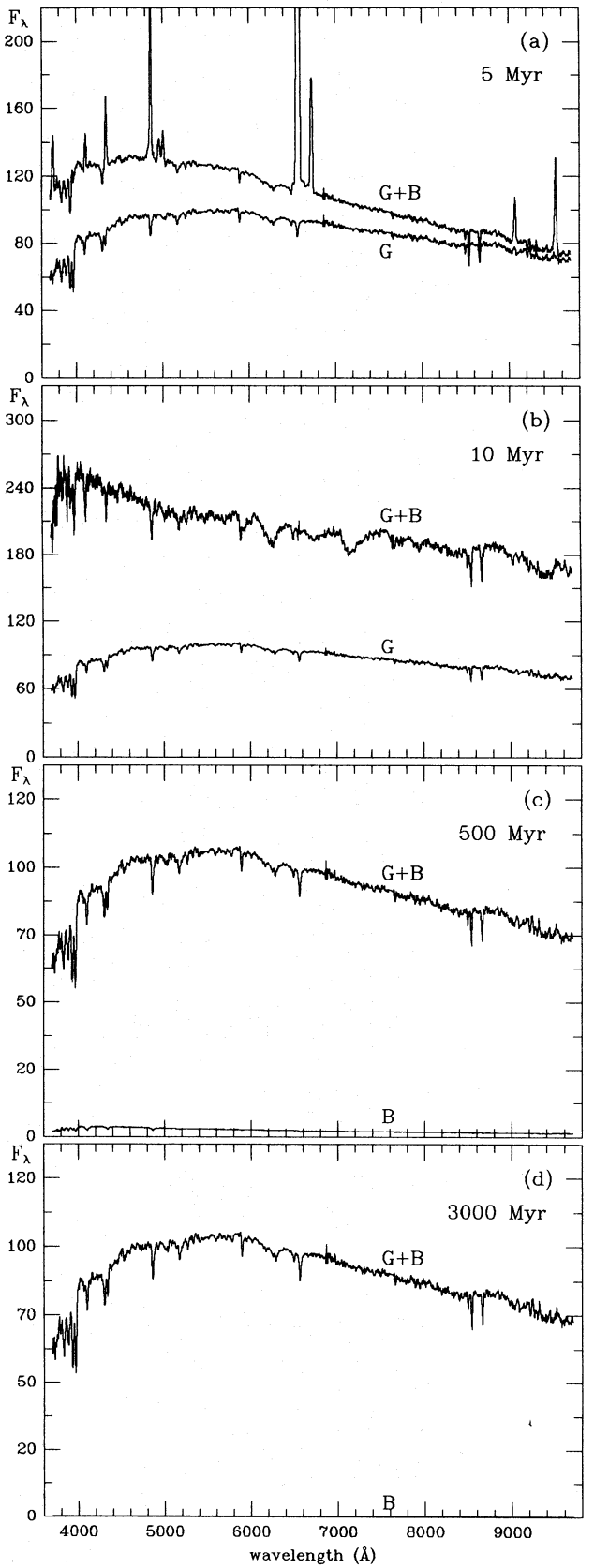

Figure 7. Same as Fig. 4 for the case of the dES template as the underlying stellar population.

Hδ, Hγ and Hβ. The equivalent widths W_λ(Å) of these features, which were obtained from the composite spectra models following the window definitions and continuum tracings as defined in Bica & Alloin (1986a, 1987a) and in Bica (1988), are provided in Table 3(a) (columns 9–16) for the case of the E4 underlying population, and in Table 3(b) for the case of the dES underlying population. As a comparison, the values of these features for pure starburst populations (RH, Y1, Y2, Y3, Y4, I1 and I2) and pure galaxy populations (E4 and dES) are listed in Table 2.

Figs 10 to 12 display the temporal behaviour of the selected lines. The metallic features show different temporal evolution between the E4 and the dES cases, as seen in Figs 10 and 11. The difference is basically caused by the differing metal abundance between the two galaxy templates. In the dES case, the metal-poor galaxy template, the CN 4216 band and the Mg I + MgH feature show (Figs 11b and 11c) only minor changes with time and practically no dependence on burst strength, as the values of these features in the galaxy template are similar to those of the star cluster templates (see Table 2). In the E4 case, the metal-rich template (Figs 10b and 10c), the galaxy feature values are stronger than those of the star clusters and therefore the dilution of these features in the composite spectrum (burst plus galaxy) can be observed as a function of both age and burst strength.

The evolution of the Ca II K line (Figs 10a and 11a) is well distinguished in both the E4 and dES cases: while this feature is strong in the galaxy templates (see Table 2), it is somewhat diluted in the cluster templates due to the blue continuum of young stars, and therefore its evolution in the composite systems can also be seen as dependent on the burst age and strength. In the case of the calcium triplet lines a distinction can be made which is related to the difference in chemical abundance of the galaxy templates and which works in the opposite way for the CN 4216 and Mg I + MgH features. We note that the feature displayed has been built from the average equivalent width between the Ca II 8542 and Ca II 8662 lines. For the E4 underlying population – the metal-rich case – the values of W_λ are close to the values of the star clusters, and the evolution of the feature shows

Table 3. Colours for galaxy-plus-starburst composite system, magnitude differences with respect to the original galaxy magnitude and equivalent widths (Å) of galaxy-plus-starburst spectra. In column 1, the model designation (G+B) specifies, for each of the three mass proportions (0.1, 1.0 and 10 per cent), the underlying galaxy (E4 or dES) and the starburst template (RH to I2).

(a) Data for the E4 underlying population case:

G+B	(B−V)	(V−R)	(V−I)	ΔB	ΔV	ΔR	ΔI	Ca II K	Hδ	CN 4216	Hγ	Hβ	Mg I+ MgH	Ca II 8542	Ca II 8662
0.1 %:															
E4+RH	0.69	0.62	1.15	-0.54	-0.31	-0.24	-0.09	7.1	-2.5	0.0	-5.3	-17.4	4.7	5.1	4.7
E4+Y1	0.58	0.59	1.34	-1.22	-0.87	-0.77	-0.84	4.8	4.3	2.4	3.8	3.7	4.4	5.9	5.1
E4+Y2	0.80	0.64	1.29	-0.28	-0.16	-0.11	-0.08	9.8	5.7	3.4	5.3	3.8	5.6	5.2	4.7
E4+Y3	0.89	0.67	1.35	-0.06	-0.04	-0.02	-0.02	12.9	4.8	3.7	5.1	3.3	6.1	5.2	4.6
E4+Y4	0.90	0.68	1.36	-0.05	-0.03	-0.02	-0.02	13.5	4.7	3.7	5.0	3.3	6.2	5.2	4.6
E4+I1	0.92	0.69	1.37	-0.01	-0.01	-0.01	0.00	13.8	4.4	3.8	4.9	3.1	6.2	5.2	4.6
E4+I2	0.92	0.69	1.37	0.00	0.00	0.00	0.00	13.9	4.4	3.8	4.9	3.1	6.3	5.2	4.6
1.0 %:															
E4+RH	0.32	0.47	0.55	-2.18	-1.58	-1.37	-0.76	0.9	-9.9	0.0	-19.5	-55.4	1.5	2.7	2.4
E4+Y1	0.39	0.51	1.31	-3.34	-2.81	-2.64	-2.75	2.3	4.2	1.8	3.4	4.0	3.2	6.3	5.5
E4+Y2	0.45	0.45	0.98	-1.50	-1.04	-0.81	-0.65	3.4	8.1	2.6	6.4	5.7	3.2	5.5	5.3
E4+Y3	0.71	0.59	1.22	-0.52	-0.31	-0.21	-0.16	8.3	6.9	3.4	6.4	4.6	5.1	5.3	4.8
E4+Y4	0.80	0.63	1.27	-0.39	-0.27	-0.21	-0.16	11.4	6.8	3.0	5.9	4.6	5.5	5.1	4.6
E4+I1	0.90	0.67	1.35	-0.09	-0.07	-0.06	-0.04	13.4	4.8	3.7	5.2	3.4	6.0	5.1	4.6
E4+I2	0.91	0.69	1.37	-0.03	-0.03	-0.03	-0.03	13.8	4.5	3.8	4.9	3.2	6.2	5.2	4.6
10.0 %:															
E4+RH	0.20	0.41	0.23	-4.55	-3.83	-3.55	-2.65	-0.4	-11.7	0.0	-23.4	-68.7	0.2	0.2	-0.3
E4+Y1	0.36	0.50	1.31	-5.79	-5.24	-5.05	-5.17	2.0	4.2	1.8	3.3	4.1	3.0	6.4	5.5
E4+Y2	0.27	0.32	0.73	-3.73	-3.08	-2.72	-2.44	1.4	8.9	2.3	6.8	6.8	1.7	5.8	5.9
E4+Y3	0.37	0.37	0.84	-2.14	-1.60	-1.28	-1.07	3.6	9.4	3.0	8.2	7.1	2.8	5.7	5.4
E4+Y4	0.56	0.49	0.99	-1.80	-1.45	-1.25	-1.07	8.1	10.4	1.7	7.7	7.3	3.8	4.7	4.8
E4+I1	0.78	0.60	1.19	-0.70	-0.56	-0.47	-0.38	11.3	6.7	3.1	6.5	4.9	4.7	4.7	4.8
E4+I2	0.88	0.67	1.36	-0.31	-0.27	-0.25	-0.25	13.1	5.1	4.1	5.4	3.7	5.5	5.1	4.7

Table 3 – *continued*

(b) Data for the dES underlying population case:

G+B	$(B-V)$	$(V-R)$	$(V-I)$	ΔB	ΔV	ΔR	ΔI	Ca II K	Hδ	CN 4216	Hγ	Hβ	Mg I+ MgH	Ca II 8542	Ca II 8662
0.1 %:															
dES+RH	0.59	0.56	1.05	-0.47	-0.30	-0.25	-0.10	4.7	-2.0	0.0	-5.0	-17.0	1.7	2.2	2.4
dES+Y1	0.52	0.55	1.28	-1.09	-0.85	-0.80	-0.89	4.0	4.1	2.0	3.6	3.7	2.7	4.8	4.4
dES+Y2	0.67	0.56	1.18	-0.24	-0.16	-0.12	-0.09	6.8	5.1	2.4	4.7	3.7	2.1	2.9	3.1
dES+Y3	0.74	0.59	1.23	-0.05	-0.03	-0.02	-0.02	8.3	4.3	2.4	4.3	3.3	2.2	2.7	2.8
dES+Y4	0.75	0.60	1.24	-0.04	-0.03	-0.02	-0.02	8.6	4.2	2.4	4.3	3.2	2.3	2.6	2.9
dES+I1	0.76	0.60	1.24	-0.01	-0.01	-0.01	0.00	8.7	4.0	2.4	4.1	3.1	2.2	2.6	2.8
dES+I2	0.76	0.60	1.25	0.00	0.00	0.00	0.00	8.7	3.9	2.4	4.1	3.1	2.2	2.6	2.8
1.0 %:															
dES+RH	0.32	0.47	0.55	-2.01	-1.55	-1.40	-0.82	0.6	-9.6	0.0	-19.1	-55.0	0.6	1.0	0.9
dES+Y1	0.39	0.51	1.30	-3.15	-2.78	-2.68	-2.83	2.3	4.2	1.8	3.4	4.0	2.9	6.1	5.3
dES+Y2	0.42	0.42	0.93	-1.36	-1.02	-0.84	-0.70	2.9	7.7	2.3	6.1	5.7	1.8	4.2	4.5
dES+Y3	0.61	0.52	1.12	-0.45	-0.30	-0.23	-0.18	6.2	6.2	2.6	5.7	4.5	2.1	3.2	3.3
dES+Y4	0.69	0.56	1.17	-0.33	-0.26	-0.22	-0.18	8.2	6.1	2.1	5.2	4.6	2.4	2.9	3.2
dES+I1	0.75	0.60	1.23	-0.08	-0.07	-0.06	-0.05	8.7	4.3	2.4	4.4	3.6	2.3	2.6	2.9
dES+I2	0.76	0.60	1.25	-0.03	-0.03	-0.03	-0.03	8.7	4.0	2.5	4.2	3.2	2.3	2.7	2.9
10.0 %:															
dES+RH	0.20	0.41	0.23	-4.35	-3.79	-3.60	-2.77	-0.4	-11.6	0.0	-23.4	-68.6	0.1	-0.2	-0.6
dES+Y1	0.36	0.50	1.31	-5.60	-5.20	-5.10	-5.26	2.0	4.2	1.8	3.3	4.1	3.0	6.4	5.5
dES+Y2	0.26	0.32	0.72	-3.54	-3.04	-2.76	-2.52	1.4	8.9	2.6	6.8	6.8	1.5	5.5	5.8
dES+Y3	0.35	0.35	0.80	-1.97	-1.57	-1.31	-1.13	3.3	9.2	2.9	8.0	7.1	1.9	4.8	4.8
dES+Y4	0.53	0.46	0.96	-1.65	-1.42	-1.28	-1.13	7.4	10.0	1.6	7.4	7.2	2.8	3.8	4.2
dES+I1	0.69	0.55	1.11	-0.61	-0.54	-0.49	-0.41	8.8	6.1	2.4	5.9	4.8	2.3	2.9	3.6
dES+I2	0.76	0.61	1.25	-0.26	-0.26	-0.26	-0.27	9.3	4.6	2.9	4.7	3.7	2.4	3.0	3.3

changes only during the early evolution of the burst (Fig. 10d), while for the dES case – the metal-poor template – the values of the features are significantly smaller than the cluster ones, and the evolution of the feature is seen to be dependent on both the age and the strength of the burst throughout its evolution (Fig. 11d). Among the metallic features, the Ca II infrared triplet is the best one to be used for deriving the metallicity of the underlying galaxy, except in the case where the starburst is younger than about 20 Myr.

The Balmer lines (Hδ, Hγ and Hβ) all have the same kind of evolution for E4 and dES and therefore only the Hβ diagram is shown in Fig. 12 for the E4 case. Among the Balmer lines, the window covering the Hβ line is the least contaminated by metallic features. The maximum value attained by this feature depends on both the age and the strength of the starbursts and therefore, together with the other Balmer features, it can easily be used to constrain these parameters in evolved starburst events in galaxies.

These diagrams demonstrate that it is a whole set of observational constraints, used in conjunction, that may bring a solution to the problem of dating mergers.

4 CONCLUDING REMARKS

We have extended to low-luminosity ellipticals ($M_V \sim -18$), and to objects in the transition between dwarf ellipticals and dwarf spheroidals ($-14 \leq M_V \leq -15$), our previous spectral simulation models for the evolution over 3 Gyr of composites built from metal-rich bulges and starbursts. For this purpose, we have used a library of galaxy and star cluster integrated spectra in the 3700–9700 Å wavelength range. The star cluster spectra have been properly scaled to represent starburst-to-galaxy mass fractions of 10, 1 and 0.1 per cent. A corresponding spectral atlas is presented, to allow the diagnosis of age and metallicity effects in the spectral evolution of a starburst superimposed on an old stellar population substratum, as observed in galaxy spectra. For more qualitative analyses, tables of *BVRI* magnitudes and related colours have been derived from these models, together with equivalent widths for a selection of metallic and Balmer features. The variation of these indices as a function of the burst age and strength is analysed, and the results can be used to study the properties of star-forming

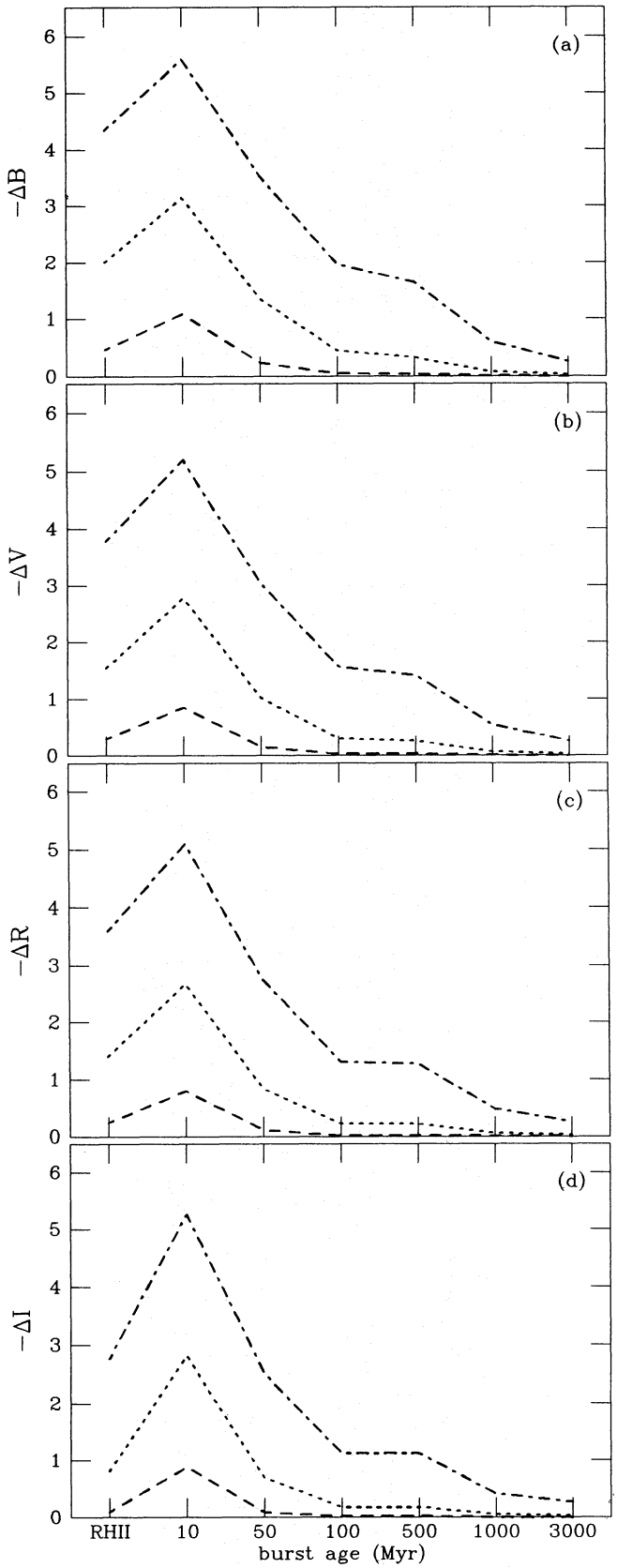

Figure 8. The increase in magnitude induced by the burst over the dES galaxy template for the *B*, *V*, *R* and *I* bands as a function of burst age and strength. Dashed line: 0.1 per cent burst-to-galaxy mass fraction; dotted line: 1 per cent; dashed-dotted line: 10 per cent.

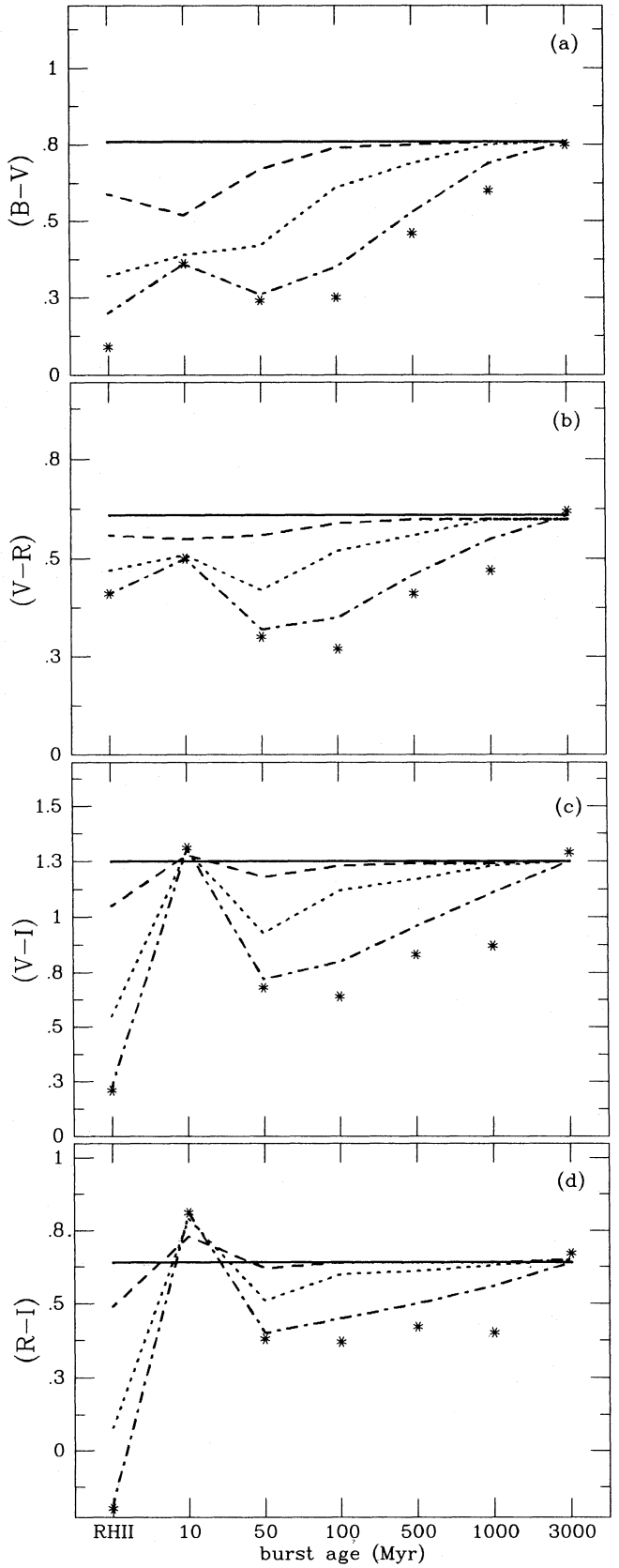

Figure 9. The $(B-V)$, $(V-R)$, $(V-I)$ and $(R-I)$ colour evolution for the composite burst plus dES template. Same line types as in Fig. 8; solid line: pure dES colour; asterisks: pure burst (star cluster) colours.

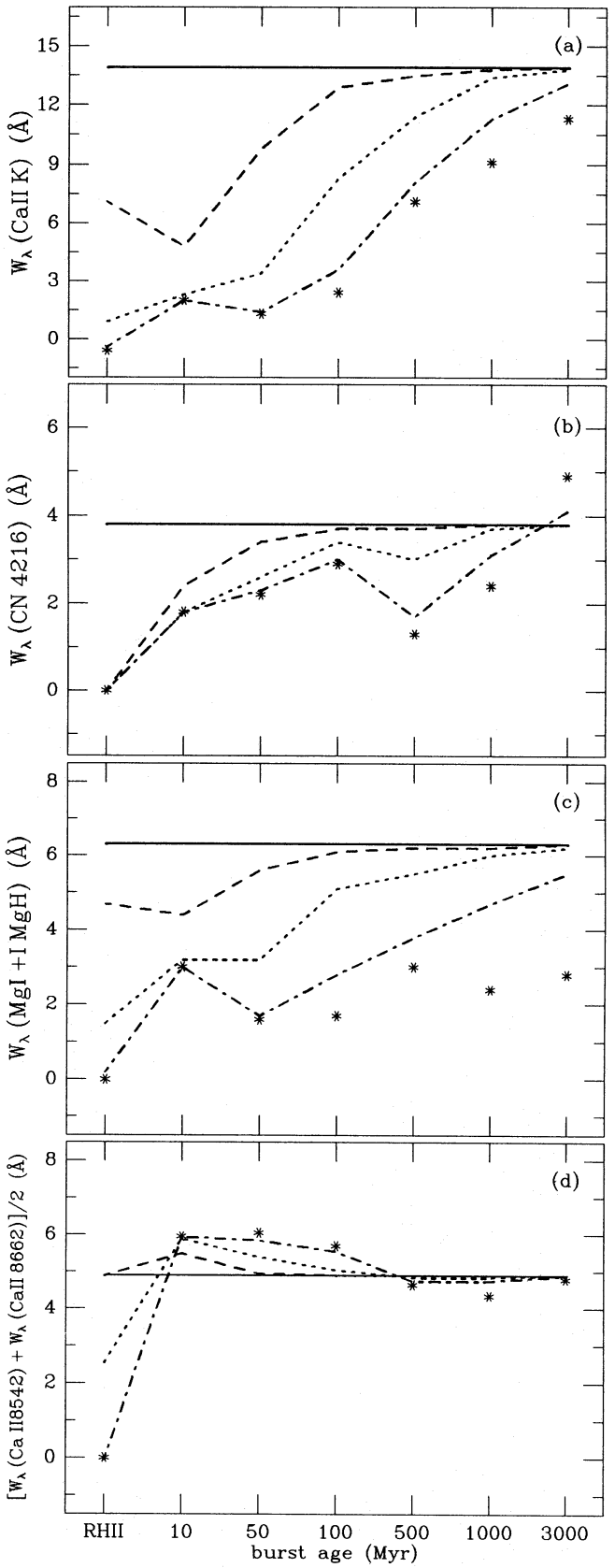

Figure 10. Evolution with time of some metallic features (W_λ) of the composite system for the E4 template case. Same symbols as in Fig. 9.

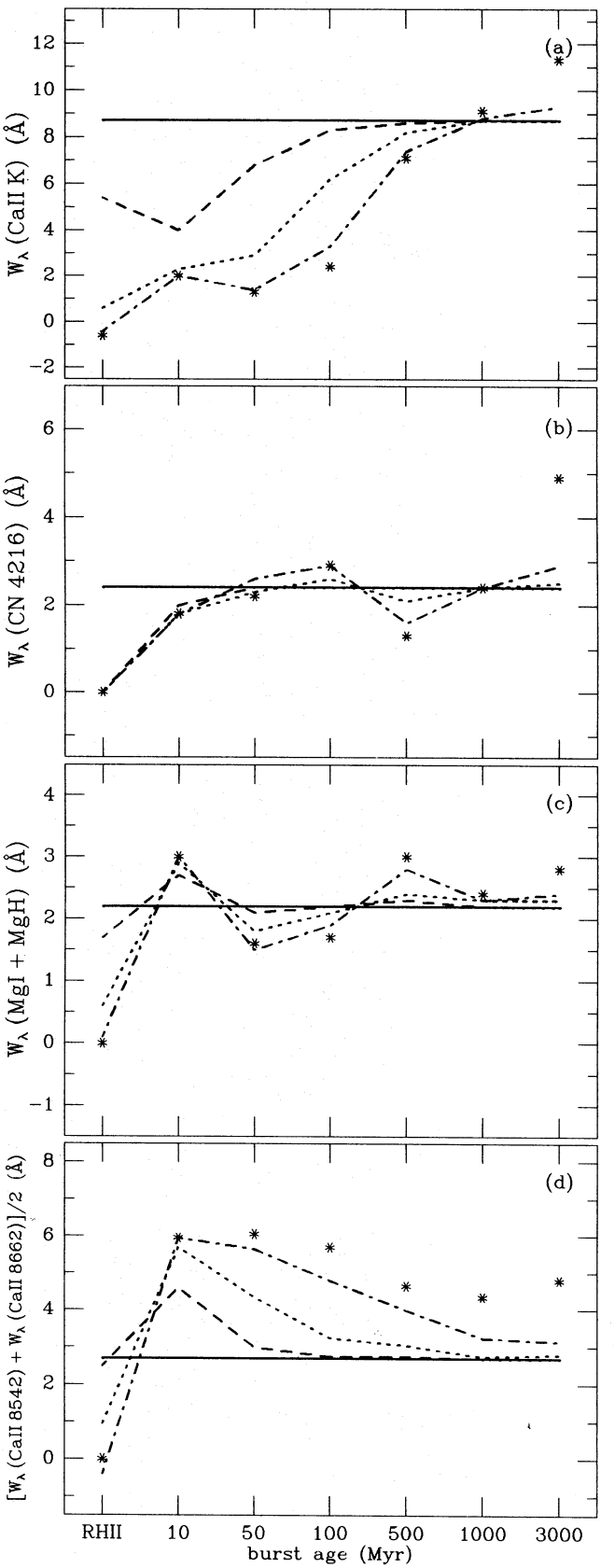

Figure 11. Same as Fig. 10 for the dES case.

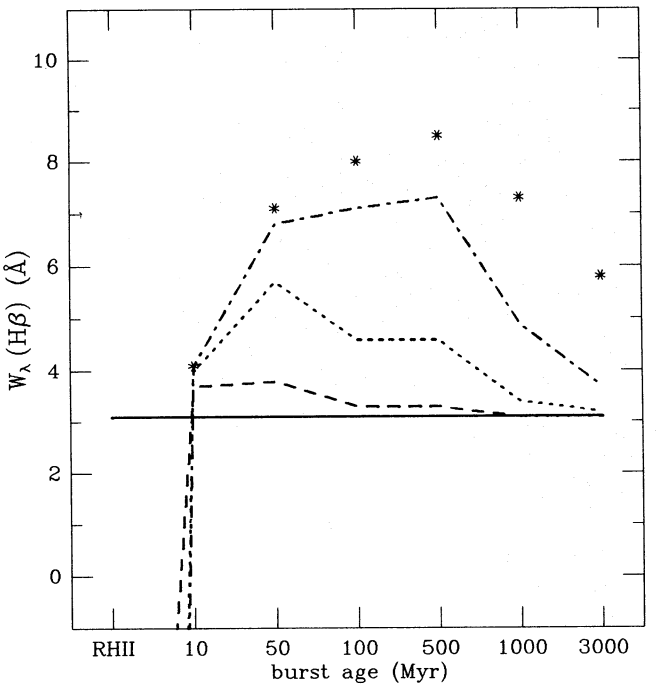

Figure 12. Evolution of the Hβ line (W_λ) as a function of age for the E4 template case. Same symbols as in Fig. 9.

events in galaxies, and eventually for dating mergers. In a forthcoming paper we will compare our model predictions with photometric and spectroscopic data on a sample of star-forming galaxies.

ACKNOWLEDGMENTS

We are indebted to the ESO staff at La Silla for their assistance during our observations. This work was supported by the Brazilian institution CNPq and the French CNRS. DA acknowledges the hospitality of ESO at the ESO Headquarters in Garching, in 1993 August, where this work was finally assembled.

REFERENCES

Arimoto N., Bica E., 1989, A&A, 222, 89
Arimoto N., Yoshii Y., 1986, A&A, 164, 260
Arimoto N., Yoshii Y., 1987, A&A, 173, 23
Ažhusenis A., Straižhis V., 1969, SvA, 13, 316
Azzopardi M., Lequeux J., 1992, in Barbuy B., Renzini A., eds, Proc. IAU Symp. 149, The Stellar Populations of Galaxies. Kluwer Academic Publishers, Doredrecht, p. 201
Bardeen J., Bond J. R., Kaiser N., Szalay A., 1986, AJ, 304, 15
Bessel M. S., 1979, PASP, 91, 589
Bessel M. S., Wickramasinghe D. T., 1979, ApJ, 227, 232
Bica E., 1988, A&A, 195, 76
Bica E., Alloin D., 1986a, A&A, 162, 21
Bica E., Alloin D., 1986b, A&AS, 66, 171
Bica E., Alloin D., 1987a, A&A, 186, 49
Bica E., Alloin D., 1987b, A&AS, 70, 281
Bica E., Arimoto N., Alloin D., 1988, A&A, 202, 8
Bica E., Alloin D., Schmidt A. A., 1990a, MNRAS, 242, 241
Bica E., Alloin D., Schmidt A. A., 1990b, A&A, 228, 23
Buonanno R., Corsi C. E., Fusi P. F., Hardy E., Zinn R., 1985, A&A, 162, 65
Charlot S., Bruzual G. A., 1991, ApJ, 367, 126
Cid-Fernandes R., Jr, Dottori H. A., Gruenwald R. B., Viegas S. M., 1992, MNRAS, 255, 165
Cousins A. W. J., 1976, Mem. R. Astron. Soc., 91, 589
Deckel A., Silk J., 1986, ApJ, 303, 39
Garcia-Vargas M. L. G., Díaz A. I., 1994, ApJS, 91, 553
Guiderdoni B., Rocca-Volmerange B., 1987, A&A, 186, 1
Gunn J. E., Stryker L. L., 1983, A&AS, 52, 121
Hensler G., Theis C., Burkert A., 1992, in Alloin D., Stasinska G., eds, The Feedback of Chemical Evolution on the Stellar Content of Galaxies. Obs. de Paris, Meudon, p. 229
Johnson H. J., 1964, Bol. Obs. Tonant. Tacub., 25, 305
Larson R. B., 1987, in Thuan T. X., Montmerle T., Van J. T. T., eds, Starbursts and Galaxy Evolution. Editions Frontières, Gif-sur-Yvette, p. 467
Larson R. B., Tinsley B. M., 1978, ApJ, 219, 46
Lee M. G., Freedman W., Mateo M., Thompson I., Roth M., Ruiz M., 1993, AJ, 106, 1420
Peebles P. J., 1987, ApJ, 315, L73
Schweizer F., Seitzer P., 1992, AJ, 104, 1039
Terlevich R., 1985, in Kunth D., Van J. T. T., eds, Starforming Dwarf Galaxies. Editions Frontières, Gif-sur-Yvette, p. 395
Yoshii Y., Arimoto N., 1987, A&A, 188, 13